Self-consistent kinetic model of the short-lived afterglow in flowing nitrogen

P A Sá[1], **V Guerra**[2], **J Loureiro**[2] **and N Sadeghi**[3]

[1] Departamento de Física, Faculdade de Engenharia, Universidade do Porto, 4200-465 Porto, Portugal
[2] Centro de Física dos Plasmas, Instituto Superior Técnico, 1049-001 Lisboa, Portugal
[3] Laboratoire de Spectrométrie Physique (UMR 5588, CNRS), Université Joseph Fourier, Grenoble, 38402 Saint-Martin d'Hères Cédex, France

Abstract
A detailed kinetic model for the flowing nitrogen microwave discharge and post-discharge is developed with the aim of gaining a deeper understanding into the processes responsible for the formation of the short-lived afterglow of nitrogen and for the enhancement of the concentration of $N_2(A\,^3\Sigma_u^+)$ metastable, measured at approximately the same position in Sadeghi *et al* (2001 *J. Phys. D: Appl. Phys.* **34** 1779). The present work shows that the peaks observed in the afterglow, for the density of molecules in radiative $N_2(B\,^3\Pi_g)$ and $N_2^+(B\,^2\Sigma_u^+)$ and metastable $N_2(A\,^3\Sigma_u^+)$ states, can be explained as a result of a pumping-up phenomenon into the vibrational ladder produced by near-resonant V–V energy-exchange collisions, involving vibrationally excited molecules $N_2(X\,^1\Sigma_g^+, v)$ in levels as high as $v \sim 35$. The present predictions are shown to be in good agreement with the measured concentrations for $N_2(A\,^3\Sigma_u^+)$ metastables and $N(^4S)$ atoms, and with the emission intensities of 1^+ and 1^- system bands of N_2.

1. Introduction

Flowing post-discharges in nitrogen-containing plasmas have been the subject of different studies in the last few years, not only to gain a better understanding of elementary processes occurring in these media but also due to the increased use of active nitrogen in remote plasma reactors for many applications. These discharges are used for steel surface nitriding [1], thin-film deposition [2, 3], plasma assisted pulsed laser deposition [4], metal surface cleaning [5] and, more recently, in bacterial sterilization [6, 7]. Accordingly, a large number of both experimental [8–13] and theoretical [14–16] works have appeared in the literature with the aim of getting a deeper insight into the understanding of the kinetics of long-lived species in these non-equilibrium media: vibrationally excited ground-electronic state $N_2(X\,^1\Sigma_g^+, v)$ and metastable $N_2(A\,^3\Sigma_u^+)$ molecules, and ground-state $N(^4S)$ and metastable $N(^2D,^2P)$ atoms. Once these species are created in the discharge region of a flowing N_2 microwave [14–16] or dc discharge [17], they may be either carried out to the post-discharge or created again in the post-discharge, as a result of a complex interplay kinetics involving other species.

Investigations in this area were initiated in the 1950s with the analysis of the formation of the well-known afterglow of nitrogen [18]. More recently, interest in this topic was rekindled through a series of spectroscopic studies [19, 20, 17], in which the emissions of the first negative system of $N_2^+(B\,^2\Sigma_u^+ \rightarrow X\,^2\Sigma_g^+)$, that is, the so-called pink afterglow, and of the first and second positive systems of nitrogen, $N_2(B\,^3\Pi_g \rightarrow A\,^3\Sigma_u^+)$ and $N_2(C\,^3\Pi_u \rightarrow B\,^3\Pi_g)$, respectively, have been recorded and analysed. Further, the role played by $N_2(X\,^1\Sigma_g^+, v)$ molecules in nitrogen afterglow has been studied in [21], and the excitation of the $N_2(B\,^3\Pi_g)$ state in [22].

Since electron impact excitation maintains some efficacy only in very early post-discharge (up to $t \sim 10^{-4}$ s) [23, 24], via stepwise excitation of $N_2(B\,^3\Pi_g)$ and $N_2(C\,^3\Pi_u)$ states from $N_2(A\,^3\Sigma_u^+)$ metastables by low energy electrons, the main energy carriers leaving the discharge and reacting in the short-lived afterglow (SLA) are the long-lived molecular and atomic species. However, the appearance of a dark zone at the end of the flowing discharge, just before the rise of the optical emissions in the SLA, indicates that the metastables $N_2(A)$ cannot be carried out from the discharge to

the post-discharge, otherwise the dark zone would not exist. The $N_2(A)$ concentration must continuously decrease until a minimum is reached in the dark zone before increasing again towards a secondary maximum placed in the SLA. This is indeed the experimental behaviour observed in [9] by using the intracavity laser absorption spectroscopy (ICLAS) technique. We notice that if the metastables $N_2(A)$ were directly transported from the discharge, the longitudinal profile of the optical emissions on 1^+, 2^+ and 1^- systems of N_2 would not decrease to a minimum in the dark zone, since the radiative states responsible for these emissions would be continuously populated and observed through the following set of reactions [14, 15]:

$$N_2(A) + N_2(X, 5 \leqslant v \leqslant 14) \rightarrow N_2(B) + N_2(X, v = 0), \quad (1)$$

$$N_2(B) \rightarrow N_2(A) + h\nu(1^+), \quad (2)$$

$$N_2(A) + N_2(A) \rightarrow N_2(C) + N_2(X, v = 0), \quad (3)$$

$$N_2(C) \rightarrow N_2(B) + h\nu(2^+), \quad (4)$$

$$N_2(A) + N_2(a') \rightarrow N_2(X, v = 0) + N_2^+(X) + e, \quad (5)$$

$$N_2(X, v \geqslant 12) + N_2^+(X) \rightarrow N_2(X, v - 12) + N_2^+(B), \quad (6)$$

$$N_2^+(B) \rightarrow N_2^+(X) + h\nu(1^-). \quad (7)$$
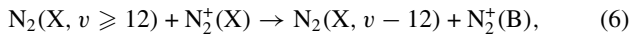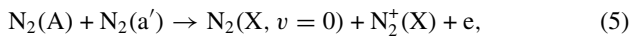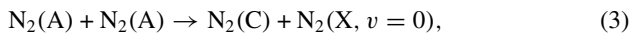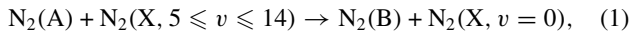
This work follows our previous publications [14–16], where we have demonstrated that the vibrationally excited molecules $N_2(X\,^1\Sigma_g^+, v)$, in levels as high as $v > 35$, should be the only energy carriers leaving the discharge capable of populating the electronic metastable $N_2(A\,^3\Sigma_u^+)$ and $N_2(a'\,^1\Sigma_u^-)$ states in the post-discharge. This is a consequence of the well-known pumping-up effect due to near-resonant vibration–vibration (V–V) energy-exchange collisions during the vibrational relaxation of anharmonic oscillators as is the case for $N_2(X\,^1\Sigma_g^+, v)$ [25], $CO(X\,^1\Sigma^+, v)$ [26, 27] and $NO(X\,^2\Pi_r, v)$ molecules [28].

In this paper, we report the results of our more recent model investigations, in which we were able to reproduce accurately and interpret the measured profiles of the $N_2(A\,^3\Sigma_u^+)$ metastable concentration using the ICLAS technique [8, 9, 12], $N(^4S)$ atom concentration by the two-photon laser-induced fluorescence (TALIF) technique [10], and of the intensity emissions of 1^+ and 1^- system bands of N_2 by optical emission spectroscopy [13]. On the other hand, the absolute density of $N_2(X\,^1\Sigma_g^+, v)$ molecules has been measured up to the level $v = 18$ by high sensitivity cavity ringdown spectroscopy (CRDS) absorption in a dc glow discharge [11]. Although the CRDS technique is very sophisticated, the level $v = 18$ is located in the Treanor plateau of the vibrational distribution function [29], which means that we are still far away from the highly vibrational levels $v > 35$ that can explain the nitrogen afterglow as a pumping-up phenomenon in the vibrational ladder. Nevertheless, the present paper clearly demonstrates that the V–V pumping-up effect is the only kinetic mechanism able to explain the spectroscopic observations in an N_2 post-discharge.

More accurate rate coefficients and a selected set of reactions are proposed in this paper relative to those presented in [15]. Also, the measured longitudinal profile for the gas temperature [9] is properly taken into account in the calculations, whereas in [15] a step function has been assumed from the discharge to post-discharge zones. Other

modifications of the model have also contributed in the attainment of a much better agreement with the experiment, such as the inclusion of a mechanism for nitrogen dissociation due to collisions between vibrationally excited molecules $N_2(X\,^1\Sigma_g^+, v)$ and $N_2(A\,^3\Sigma_u^+)$ metastables [30, 31], as well as the detailed description of the kinetics of atomic metastable species $N(^2D)$ and $N(^2P)$ [32]. Finally, the possibility of other explanations and reaction paths [9, 15] is also discussed and evaluated in the present analysis.

2. Modelling details

The kinetic model used in this paper has two separate modules, one for the discharge in the microwave field (I) and another for the post-discharge (II), the stationary solutions obtained in I being the initial conditions for module II.

Regarding the discharge module, the electron energy distribution function (EEDF), the vibrational distribution function (VDF) of $N_2(X\,^1\Sigma_g^+, v)$ molecules, the concentrations of N_2 electronic states ($A\,^3\Sigma_u^+$, $B\,^3\Pi_g$, $B'\,^3\Sigma_u^-$, $C\,^3\Pi_u$, $a'\,^1\Sigma_u^-$, $a\,^1\Pi_g$, $w\,^1\Delta_u$), of ground and excited atoms $N(^4S, {}^2D, {}^2P)$, and of $N_2^+(X\,^2\Sigma_g^+, B\,^2\Sigma_u^+)$ and N_4^+ ions, are obtained from the coupled solutions to the stationary homogeneous electron Boltzmann equation for the microwave field, using the effective-field approximation, coupled to a system of stationary rate-balance equations for the neutral and charged heavy species. Additionally, the maintenance of a high-frequency electric field is self-consistently determined in the framework of the present model by assuming the exact balance, under steady-state conditions, between the total rate of ionization and the total rate of electron losses by ambipolar diffusion plus electron–ion recombination. The reader should refer to the following references for details about this model: electron Boltzmann equation and determination of the EEDF [29, 33]; kinetics of $N_2(X\,^1\Sigma_g^+, v)$ molecules [29]; kinetics of N_2 electronic states and field maintenance [34]; nitrogen discharge sustained by a microwave field [14]. Nevertheless, two important modifications have been introduced in this paper compared to our previous work [15] devoted to nitrogen afterglow:

(i) The kinetics of atomic metastables $N(^2D)$ and $N(^2P)$ have been included in the model using the same set of reactions as in [32], which allows us to consider, as pointed out in [9], the conjoint action of the strongly correlated mechanisms with an important role in the SLA

$$N_2(A) + N(^4S) \rightarrow N_2(X, 6 \leqslant v \leqslant 9) + N(^2P), \quad (8)$$

$$N_2(X, v \geqslant 10) + N(^2P) \rightarrow N_2(A) + N(^4S). \quad (9)$$
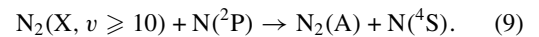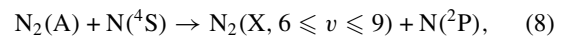
(ii) Besides dissociation by electron impact, a channel for dissociation of N_2 has been assumed as well via an excitation mechanism to the predissociative levels $N_2(B\,^3\Pi_g, v' \geqslant 13)$ [31]

$$\begin{aligned} N_2(X, 15 \leqslant v \leqslant 19) &+ N_2(A) \\ &\rightarrow N_2(X, v = 0) + N_2(B, v' \geqslant 13) \\ &\rightarrow N_2(X, v = 0) + N(^4S) + N(^4S). \end{aligned} \quad (10)$$
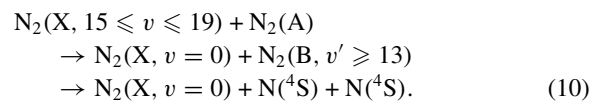
Reactions (8) and (9) have been considered in this paper with the rate coefficients $k_8 = 4 \times 10^{-11}\,\mathrm{cm^3\,s^{-1}}$ [35] and

$k_9 = 10^{-10} \times \exp(-1300/T_g) \, \mathrm{cm^3 \, s^{-1}}$ [36], with T_g denoting the gas temperature in K. For $T_g = 1000$ K assumed in this paper for a microwave discharge, we obtain $k_9 = 2.7 \times 10^{-11} \, \mathrm{cm^3 \, s^{-1}}$. This value is not far from that proposed in [9], $4 \times 10^{-11} \, \mathrm{cm^3 \, s^{-1}}$, based on a balance between reactions (8) and (9) and by the absence of any energy barrier for both reactions.

Reaction (10) has been seen to be an important source of N(^{4}S) atoms in a dc nitrogen discharge, produced in an S-52 glass cylindrical tube with inner radius $R = 7.5$ mm, for pressures $p > 100$ Pa and discharge currents $I > 50$ mA [30, 31]. See also [37] about the need to use such a reaction in a non-self-sustained nitrogen glow discharge. However, reaction (10) does not provide a good explanation of the experimental results at lower discharge currents. In this latter case it was seen that a different mechanism involving collisions between two vibrationally excited molecules [31, 38, 39]

N$_2$(X, 10 < v < 25) + N$_2$(X, 10 < v < 25)
$$\to \mathrm{N_2(X}, v = 0) + \mathrm{N}(^4\mathrm{S}) + \mathrm{N}(^4\mathrm{S}) \qquad (11)$$
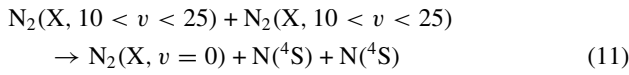
needs to be used together with reaction (10), besides dissociation by electron impact.

Under the conditions of the present work, corresponding to a nitrogen microwave discharge at $\omega/(2\pi) = 433$ MHz and $p = 440$ Pa, in an $R = 1.9$ cm tube radius, the electron density and the degree of vibrational excitation are close to the values for which reaction (10) prevails. Hence, process (10) has been assumed here with the rate coefficient $k_{10} = 1.5 \times 10^{-12} \, \mathrm{cm^3 \, s^{-1}}$ [30, 31], which is a value of about one order of magnitude smaller than the rate coefficient for the excitation of N$_2$(B$^3\Pi_g$, $v' \leqslant 12$) levels in collisions between N$_2$(X$^1\Sigma_g^+$, $5 \leqslant v \leqslant 14$) molecules and N$_2$(A$^3\Sigma_u^+$) metastables, $2 \times 10^{-11} \, \mathrm{cm^3 \, s^{-1}}$ [32, 40]. On the other hand, the electron dissociation cross-section used has been taken from [41] through a total dissociation cross-section that considers, among other channels, the excitation of predissociative levels N$_2$(B$^3\Pi_g$, $v' > 12$), N$_2$(C$^3\Pi_u$, $v' > 4$) and N$_2$(a$^1\Pi_g$, $v' > 6$). Basically, the inclusion of process (10) in this paper has two consequences: (i) it provides an enhancement of the concentration of N(^{4}S) atoms to values in agreement with the measurements realized in [10], since the comparison with that paper has been used here, in parallel with [9], to validate the mechanisms proposed to explain the nitrogen afterglow; (ii) it produces a reduction of the concentration of N$_2$(A$^3\Sigma_u^+$) metastables to values close to those reported in [9], due to an increase in the effects of reaction (8) for quenching of N$_2$(A) by N(^{4}S) atoms.

Since the concentrations of N(^{4}S) atoms are larger than those usually obtained assuming dissociation by electron impact only, the effect of vibrational deactivation of N$_2$(X$^1\Sigma_g^+$, v) molecules by vibration–translation (V–T) energy exchange processes in collisions with N(^{4}S) atoms is also enhanced. Accordingly, we have found a need to reduce the rate coefficients of V–T(N$_2$–N) processes by a factor $\times 1/5$ with respect to the data reported in [42, 43], which were used in our previous publication [15]. As before, multi-quantum transitions from one to five quanta have been considered.

These are basically the modifications operated in the model compared to our previous works. In doing so, the present model constitutes a powerful predictive tool that is able to determine the concentrations of the various active species in a nitrogen microwave discharge. Once the concentrations are determined in the discharge, their time-evolution in the post-discharge can be easily studied by considering the relaxation of the set of coupled kinetic master equations. As discussed in [23], the electron collisions in the post-discharge, although not absolutely vanishing, cannot be responsible for the enhancement of the optical emissions on the 1$^+$ and 1$^-$ systems of N$_2$ and of N$_2$(A$^3\Sigma_u^+$) concentration in the afterglow [9, 19, 20]. Electron impact processes are therefore neglected in the post-discharge with the exception of the case of electron–ion recombination of N$_2^+$ ions, for which a measured $n_e(z)$ profile has been used [9]. The electron–ion recombination mechanism for N$_2^+$(X$^2\Sigma_g^+$) in the post-discharge has been revealed to be very important, together with ambipolar diffusion, at the moment of determining the concentration of the upper ionic species N$_2^+$(B$^2\Sigma_u^+$) responsible for the emission of the 1$^-$ system of N$_2$.

The set of reactions taken into account in the relaxation model for the post-discharge is basically the same as in the discharge, with the inclusion of a few new reactions. As discussed in [14–16], the appearance of a brightened zone downstream from the flowing discharge, in the SLA region, clearly separated by a dark zone from the power-input region, can only be explained by considering collisional processes involving highly excited vibrational levels N$_2$(X$^1\Sigma_g^+$, v).

In fact, due to the anharmonicity of the potential energy curve of N$_2$(X$^1\Sigma_g^+$) the V–V energy exchanges of the type

$$\mathrm{N_2(X}, v) + \mathrm{N_2(X}, w) \to \mathrm{N_2(X}, v-1) + \mathrm{N_2(X}, w+1) \quad (12)$$
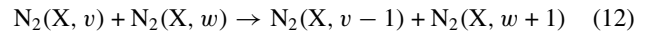
are not exactly resonant and generate an increase in quanta in the vibrational ladder as the electron–vibration (e–V) processes are cut off [25]. This effect, which also exists for other diatomic molecules, such as CO(X$^1\Sigma^+$) [26, 27] and NO(X$^2\Pi_r$) [28], is of great importance in molecular lasers, supersonic gas flows and in the upper atmosphere. In the case of N$_2$ discharges, vibrationally excited molecules N$_2$(X$^1\Sigma_g^+$, v), in levels as high as $v \sim 35$, are strongly populated during the relaxation processes. These levels can lead to the formation of N$_2$(A$^3\Sigma_u^+$) and N$_2$(a$'^1\Sigma_u^-$) states as a result of collisions between vibrationally excited molecules and ground-state N(^{4}S) atoms:

$$\mathrm{N_2(X}, v \geqslant 39) + \mathrm{N}(^4\mathrm{S}) \to \mathrm{N_2(A)} + \mathrm{N}(^2\mathrm{D}), \qquad (13)$$

$$\mathrm{N_2(X}, v \geqslant 38) + \mathrm{N}(^4\mathrm{S}) \to \mathrm{N_2(a')} + \mathrm{N}(^4\mathrm{S}). \qquad (14)$$
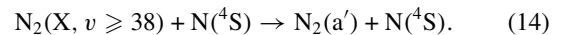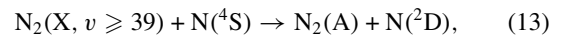
Mechanisms of this type, for the creation of electronically excited states by collision-induced resonant vibration–electronic (V–E) energy transfer, were experimentally observed in CO(X$^1\Sigma^+$, v) [27, 44] and suggested for NO(X$^2\Pi_r$, v) [28, 45]. Other reactions investigated in [15] for N$_2$(X, v) involving lower vth levels have not been considered here since they do not obey the spin conservation rules and, further, they predict broader peaks for the species concentrations in the SLA.

Although reactions (13) and (14) are allowed by spin conservation, the corresponding rate coefficients are unknown. Here, we will consider $k_{13} = k_{14} = 10^{-11} \, \mathrm{cm^3 \, s^{-1}}$ by comparing the calculations to the experimental data [9], but the influence of using other values will be discussed as well. The ground-state N(^{4}S) atoms are long-lived species with their

relative concentrations practically constant in the afterglow up to $t \sim 10^{-1}$ s. Indeed, the absolute concentration [N(^{4}S)] increases due to the temperature decrease in the post-discharge.

Once the species N$_2$(A$^3\Sigma_u^+$) and N$_2$(a$'^1\Sigma_u^-$) are created in the afterglow, the optical emissions of the 1$^+$, 2$^+$ and 1$^-$ systems of N$_2$ can take place through reactions (1)–(7). In the case of the 1$^-$ system, the upper ionic species N$_2^+$(B$^2\Sigma_u^+$) is created by reaction (6) involving collisions of N$_2$(X$^1\Sigma_g^+$, $v \geqslant 12$) levels with N$_2^+$(X$^2\Sigma_g^+$) ions, the latter being created in the afterglow by the Penning ionization reactions (5) and

$$N_2(a') + N_2(a') \rightarrow N_2(X, v = 0) + N_2^+(X) + e. \quad (15)$$
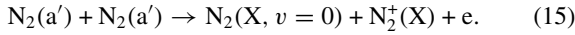
Reactions (5) and (15) are also very important in the discharge zone, since their ionization rates can be larger than the rates for ionization by electron impact [46], typically for $p > 100$ Pa. In contrast, reactions (13) and (14) do not play a significant role in the discharge due to the vanishing concentrations of the high vibrational levels, $v > 35$, of the VDF at discharge conditions [29].

This paper is concerned only with the kinetics of neutral and charged heavy-species in the afterglow. Obviously, reactions (5) and (15) produce an increase in the electron density as well, which was seen to be in agreement [16, 24] with the measurements reported in [9]. The reader should refer to [23, 24] for details on the time-dependence of the EEDF and the electron density in a nitrogen post-discharge by solving the time-dependent Boltzmann equation. In those papers, the effect of other mechanisms leading to electron production in the post-discharge has also been checked, that is

$$N_2(X, v \geqslant 30) + N_2(a') \rightarrow N_2(X, v = 0) + N_2^+(X) + e, \quad (16)$$

$$N_2(X, v \geqslant 36) + N_2(B) \rightarrow N_2(X, v = 0) + N_2^+(X) + e, \quad (17)$$
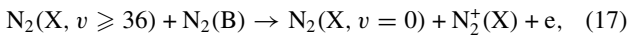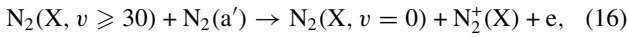
but their effects have been seen to be always vanishingly small.

3. Results and discussion

3.1. Reference model

The results have been obtained for the same conditions as in [8–10], which correspond to a flowing microwave discharge operating at $\omega/(2\pi) = 433$ MHz, in a Pyrex tube with inner radius $R = 1.9$ cm, $p = 440$ Pa and flow rate $Q = 1.5$ slpm. The electron density in the discharge and beginning of the afterglow has been assumed $n_e(0) = 3 \times 10^{10}$ cm^{-3} according to [9], while for the gas temperature we have considered $T_g = 1000$ K in the discharge and the variation $T_g(z)$ measured in [9] for the post-discharge. As discussed in [8, 9], the gas temperature is assumed equal to the rotational temperature measured for N$_2$(A$^3\Sigma_u^+$, $v' = 0$) molecules. The temperature profile shown in [9] presents a strong temperature drop at the beginning of the afterglow ($z \sim 4$ cm), a value of about $T_g \sim 500$ K at the position of the maximum of intensities in the afterglow ($z \sim 19$ cm) and tending to room temperature in the late afterglow. Under the present conditions, the pressure gradient is weak, i.e. the product of the gas density by the gas temperature is practically constant. The conversion between afterglow distances and times has been calculated assuming constant mass flow, which corresponds to a constant ratio of the

velocity of the molecules to the gas temperature, and therefore to an afterglow time at z position given by

$$t(z) = \frac{T_g(0)}{v(0)} \int_0^z \frac{dz'}{T_g(z')}. \quad (18)$$

The value of $n_e(0) = 3 \times 10^{10}$ cm^{-3} used here has been estimated in [9] and is slightly larger than the critical value for surface wave mode propagation at 433 MHz, $n_{ec} = 1.17 \times 10^{10}$ cm^{-3}. On the other hand, the value of n_e in the discharge was estimated to be $n_e = 10^{11}$ cm^{-3}, in agreement with the microwave power supplied to the discharge of 300 W and discharge length 8 cm [9, 14].

Besides the gas temperature variation along the post-discharge measured in [9], the measured profile for the electron density $n_e(z)$ has also been used in the model to take into account the losses of N$_2^+$(X$^2\Sigma_g^+$) ions by electron–ion recombination, with a rate coefficient $\alpha = 4.8 \times 10^{-7} \times (300/T_e)^{1/2}$ [47], in which T_e in K is assumed to have the same value as that of the vibrational temperature of N$_2$(X$^1\Sigma_g^+$, v) molecules in the discharge. Moreover, dependences on the gas temperature along the post-discharge were used for various rate coefficients, such as those of V–V and V–T processes [29, 42, 43], the three-body atomic recombination coefficients for populating N$_2$(B$^3\Pi_g$) and N$_2$(a$^1\Pi_g$) states [47–50]

$$N(^4S) + N(^4S) + N_2 \rightarrow N_2(B) + N_2, \quad (19)$$

$$N(^4S) + N(^4S) + N_2 \rightarrow N_2(a) + N_2 \quad (20)$$
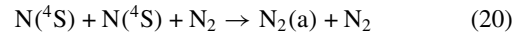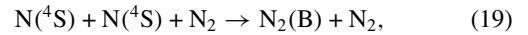
and the recombination probability of N(^{4}S) atoms on the wall, γ [48, 51].

Figures 1–3 show the comparison between the present model predictions and the measured data [9, 12, 13] for the temporal evolution of the fractional concentrations
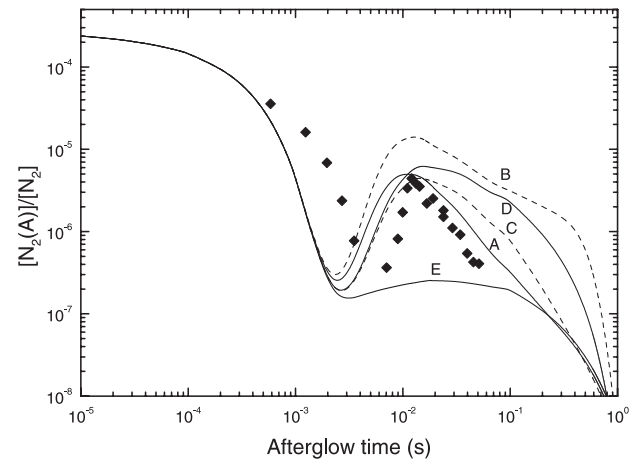
Figure 1. Temporal evolution of the fractional concentration of the N$_2$(A) metastable, in the afterglow of a microwave discharge at $\omega/(2\pi) = 433$ MHz with $p = 440$ Pa and $Q = 1.5$ slpm, assuming the formation of N$_2$(A) and N$_2$(a$'$) through the mechanisms N$_2$(X, $v \geqslant 39$) + N(^{4}S) → N$_2$(A) + N(^{2}D), reaction (13) (see text), and N$_2$(X, $v \geqslant 38$) + N(^{4}S) → N$_2$(a$'$) + N(^{4}S), reaction (14), with the rate coefficients in cm^3 s^{-1}: (A) $k_{13} = k_{14} = 10^{-11}$; (B) $k_{13} = 10^{-11}$ and $k_{14} = 10^{-12}$; (C) $k_{13} = k_{14} = 10^{-12}$; (D) $k_{13} = 10^{-12}$ and $k_{14} = 10^{-13}$; (E) $k_{13} = k_{14} = 0$. The experimental data are from [9], multiplied by a correction factor 5 [12].
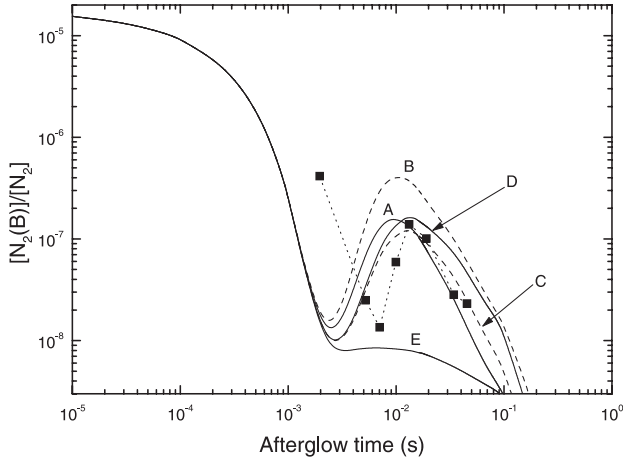
Figure 2. Fractional concentration of $N_2(B)$ radiative state for the same conditions and notation as in figure 1. The data points report concentrations in arbitrary units obtained from emission spectroscopy of the nitrogen 1^+ system bands [13].
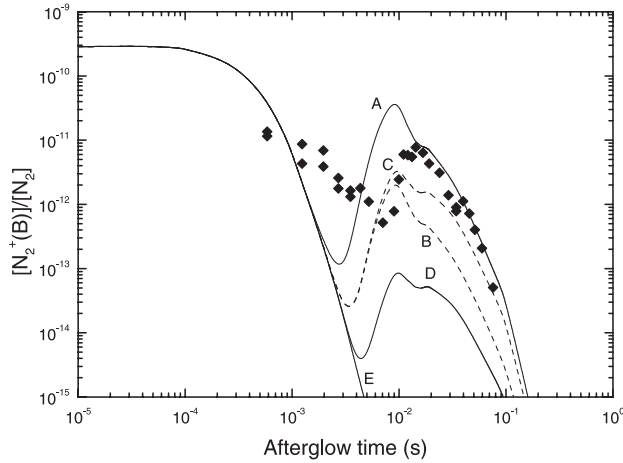
Figure 3. Fractional concentration of the upper ionic species $N_2^+(B)$ for the same conditions and notation as in figure 1. The data points represent the concentrations obtained from emission spectroscopy of the 1^- system bands of N_2 [13].

of $N_2(A\,^3\Sigma_u^+)$ metastables and $N_2(B\,^3\Pi_g)$ and $N_2^+(B\,^2\Sigma_u^+)$ radiative states in the afterglow of a microwave discharge for the conditions reported above. The different curves are for the following combinations of the rate coefficients of reactions (13) and (14): $k_{13} = 10^{-11}\,\mathrm{cm^3\,s^{-1}}$, $k_{14} = 10^{-11}\,\mathrm{cm^3\,s^{-1}}$ (A); $10^{-11}\,\mathrm{cm^3\,s^{-1}}$, $10^{-12}\,\mathrm{cm^3\,s^{-1}}$ (B); $10^{-12}\,\mathrm{cm^3\,s^{-1}}$, $10^{-12}\,\mathrm{cm^3\,s^{-1}}$ (C); $10^{-12}\,\mathrm{cm^3\,s^{-1}}$, $10^{-13}\,\mathrm{cm^3\,s^{-1}}$ (D); 0, 0 (E). The experimental data have been obtained using the ICLAS technique in the case of $[N_2(A, v' = 0\text{–}6)]$ absolute concentration [12] and emission spectroscopy of the nitrogen 1^+ and 1^- system bands for relative measurements of the concentrations of $N_2(B)$ and $N_2^+(B)$ states [13]. Figures 1–3 show that there exists excellent agreement between theory and experiment for the position of the maximum at $\sim 15\,\mathrm{ms}$ occurring in the SLA. This constitutes a large improvement compared to our previous predictions where only qualitative agreement had been achieved [14, 15]. Note that there is a difference of a factor of 5 between the measured total population of the $N_2(A, v' = 0\text{–}6)$ state, as reported in [12], and the
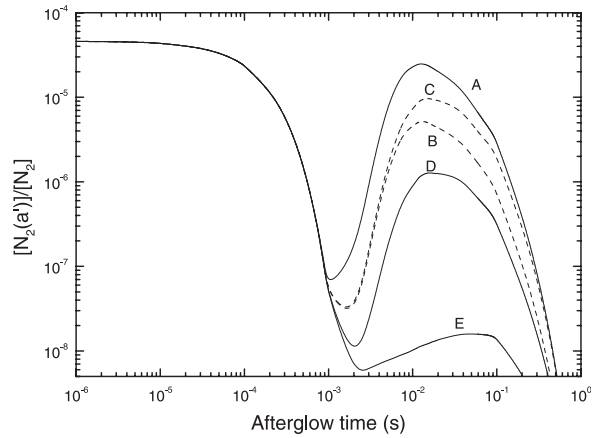
concentration of $N_2(A, v' = 0)$, previously given in [9]. Even if the general agreement between model predictions and measurements for $t \sim 10^{-4}\text{–}10^{-2}\,\mathrm{s}$ is rather satisfactory, some discrepancies do exist. One possible reason for these discrepancies is that we have not treated the various vibrational levels of each electronic state in detail, but we have considered, instead, a total population for each state. We recall here that we have used collisional data from our previous models [14, 32, 34] with a minimum number of modifications. In particular, we have only made a single adjustment, related to the rate coefficients for V–T(N_2–N) collisions, and have further included reactions (10), (13) and (14). A different possibility for the observed discrepancy may be related to the absence in the model of reactions of the type of (13) and (14) but with the presence of electrons instead of N(^{4}S) atoms, as experimentally observed for CO in [27], such as

$$e(\epsilon + \Delta\epsilon) + N_2(X, v) \rightarrow e(\epsilon) + N_2(A, B, a').$$
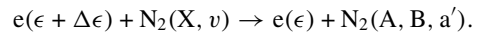
We note that the electron density profile in the afterglow is very narrow, while that of N(^{4}S) atoms is flat; thus, the inclusion of these electron processes will surely tend to narrow the maxima for the different concentrations.

The increase in $[N_2(A)]$ and $[N_2(B)]$ concentrations from curve A to curve B, as the rate coefficient k_{14} decreases from $10^{-11}\,\mathrm{cm^3\,s^{-1}}$ to $10^{-12}\,\mathrm{cm^3\,s^{-1}}$, is a consequence of an enhancement of the tail of the VDF due to a smaller efficiency of reaction (14) in destroying the vth levels. This fact allows larger concentrations of $N_2(A)$ and $N_2(B)$ states to be obtained as we pass from curve A to curve B, keeping the value of k_{13} constant. In contrast, in the case of the $N_2^+(B)$ state its concentration is obtained through reactions (5) and (15) of Penning ionization followed by reaction (6), reactions (5) and (15) being strongly dependent on the $[N_2(a'\,^1\Sigma_u^-)]$ concentration. For completeness, figure 4 presents the relative concentration of the $N_2(a')$ state calculated under the same conditions as before, in which we can see that the largest concentrations correspond to $k_{14} = 10^{-11}\,\mathrm{cm^3\,s^{-1}}$ since process (14) directly populates $N_2(a')$. The measurement of $N_2(a')$ concentrations will be published in a future work.

This study clearly shows that the vibrationally excited molecules $N_2(X\,^1\Sigma_g^+, v)$ in levels $v > 35$ are the only energy carriers leaving the discharge capable of producing electronic

Figure 4. Calculated fractional concentration of the $N_2(a')$ metastable for the same conditions and notation as in figure 1.

225
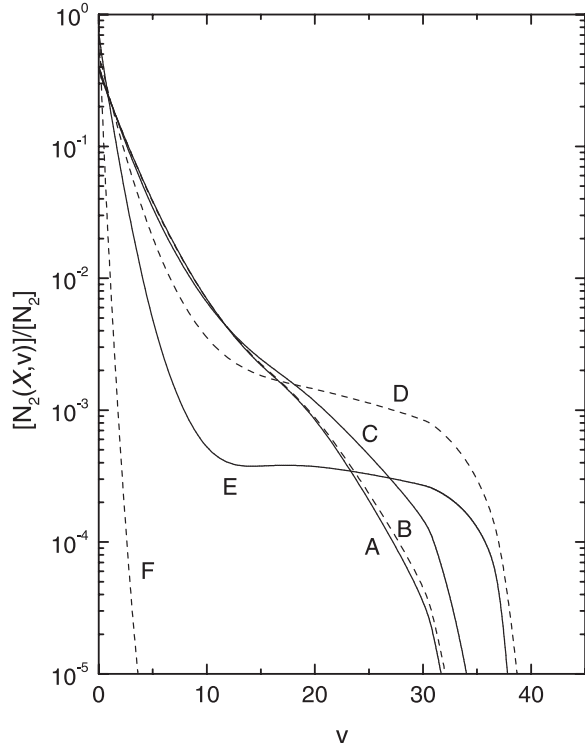
Figure 5. Vibrational distribution function of $N_2(X, v)$ molecules calculated under the conditions of curve A in figure 1, at different instants in the afterglow: (A) $t = 0$; (B) 10^{-4} s; (C) 10^{-3} s; (D) 10^{-2} s; (E) 10^{-1} s; (F) 1 s.

metastables in the post-discharge, as a consequence of the V–V pumping-up effect. If other mechanisms were considered, which involved lower v levels, such as reactions previously considered in [15]

$$N_2(X, v \geqslant 12) + N_2(X, v \geqslant 12) \rightarrow N_2(A) + N_2(X, v = 0), \tag{21}$$

$$N_2(X, v \geqslant 25) + N(^4S) \rightarrow N_2(A) + N(^4S), \tag{22}$$
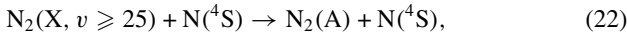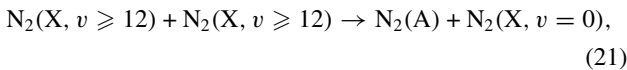
the maximum obtained in the afterglow would be much flatter [15]. Further, these reactions do not obey the spin conservation rules; hence, we believe that they should be very inefficient.

The pumping-up effect on the vibrational ladder can be well understood through figure 5, in which the VDF of $N_2(X\,^1\Sigma_g^+, v)$ molecules is calculated, under the conditions of curve A in figures 1–4, for the following instants in the post-discharge: $t = 0$ (A); 10^{-4} s (B); 10^{-3} s (C); 10^{-2} s (D); 10^{-1} s (E); 1 s (F). The tail of the VDF passes through a maximum in the conditions of curve D, $t = 10^{-2}$ s, which agrees well with the instant of appearance of the maxima for the species concentrations in the SLA. The high-sensitivity CRDS absorption technique has been used in [11] to measure the absolute density of $N_2(X, v)$ molecules in the $v = 18$ level in a dc glow discharge at $p = 300$ Pa and $I = 100$ mA. Although the level $v = 18$ is located in the Treanor plateau of the VDF and hence cannot be used to confirm the shape of the VDF at higher v levels, the measurement at $v = 18$ is in very good agreement with the present calculations [16]. To reinforce this analysis we plot in figure 6, as a function of time, the populations of some particular vibrational levels $N_2(X, v)$, for $v = 10, 20, 30, 35, 40$ and 45, normalized to
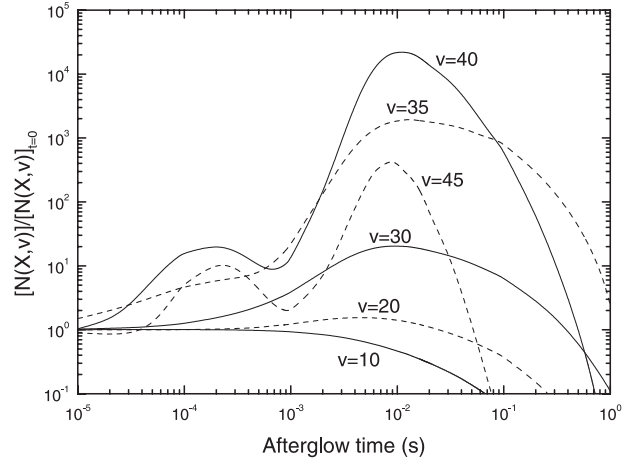
Figure 6. Temporal evolution of the relative population of some particular vibrational levels in VDF, normalized to their population at $t = 0$, calculated under the conditions of curve A in figure 1.
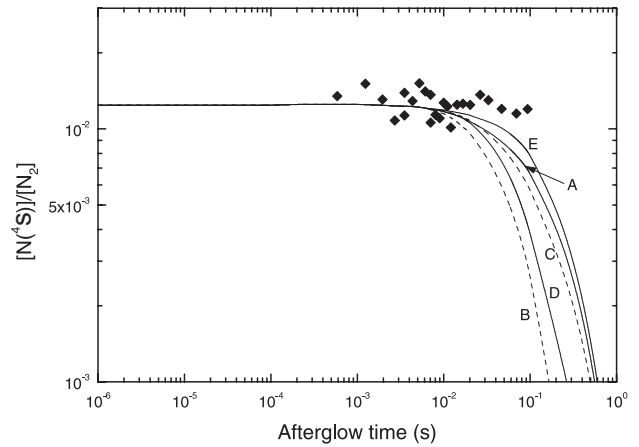
Figure 7. Temporal evolution of the fractional concentration of $N(^4S)$ atoms for the same conditions and notation as in figure 1. The experimental data are from [10].

their concentration at the beginning of the afterglow. This figure shows that only the highest v levels, typically larger than $v \sim 35$, exhibit the correct profile that can explain the appearance of the observed peaks in the SLA.

Figure 7 shows the calculated relative concentrations of $N(^4S)$ atoms, for the same combinations of the rate coefficients of reactions (13) and (14) as in figures 1–4, together with measured data obtained using the TALIF technique [10]. The agreement between theory and experiment is quite good in the range 10^{-3}–10^{-1} s, the time point at which the concentration of $N(^4S)$ atoms starts to decrease as a result of the reassociation on the wall and three-body recombination. The calculated lifetime of nitrogen atoms may look short at first sight, since it is known that the recombination of $N(^4S)$ atoms can last for a very long time. However, for the present conditions, even if we assume that $N(^4S)$ atoms do not participate in any chemistry and are lost only at the wall with a probability $\gamma \sim 3 \times 10^{-6}$ s [48], we easily obtain a characteristic lifetime only of the order of ~ 10 s. The fractional concentration $[N(^4S)]/[N_2]$ remains unchanged up to $\sim 5 \times 10^{-2}$ s, so that the observed peaks for the relative concentrations of $N_2(A\,^3\Sigma_u^+)$, $N_2(B\,^3\Pi_g)$ and $N_2^+(B\,^2\Sigma_u^+)$ states essentially reflect the behaviour found
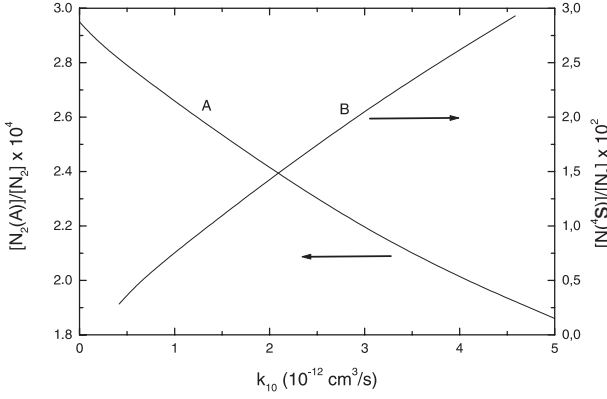
Figure 8. Fractional concentration of $N_2(A)$ metastables (curve A) and $N(^4S)$ atoms (curve B), as a function of the rate coefficient of the dissociation reaction (10): $N_2(X, 15 \leqslant v \leqslant 19) + N_2(A) \rightarrow N_2(X, v = 0) + N(^4S)$, under the conditions of figure 1 and $n_e(0) = 3 \times 10^{10}\,\mathrm{cm}^{-3}$.

Figure 9. As in figure 8 but as a function of the electron density in the discharge. The rate coefficient of the dissociation reaction (10) is our standard value $k_{10} = 1.5 \times 10^{-12}\,\mathrm{cm}^3\,\mathrm{s}^{-1}$.

for the time evolution of $N_2(X\,^1\Sigma_g^+, v > 35)$ molecules. Note that even if the concentration of the $N(^4S)$ atoms is relatively high, under the conditions used in this work the state $N_2(B\,^3\Pi_g)$ is nevertheless formed essentially via reaction (1), the contribution of the three-body reaction (19) being negligible (see also figure 11).

The agreement between measured and predicted concentrations of $N(^4S)$ atoms is a consequence of the magnitude chosen for the rate coefficient of the dissociation reaction (10). Here, we have considered $k_{10} = 1.5 \times 10^{-12}\,\mathrm{cm}^3\,\mathrm{s}^{-1}$, but the effects produced by using other values for k_{10} in the discharge may be analysed in figure 8. An increase in the rate coefficient k_{10} produces both an increase in the rate of dissociation and, to a much lesser extent, a decrease in the concentration of the $N_2(A\,^3\Sigma_u^+)$ metastable due to the enhancement of the quenching process by $N(^4S)$ atoms (8). We note that this latter reaction is balanced by reaction (9), which recycles $N_2(A\,^3\Sigma_u^+)$ molecules.

Finally, it would also be interesting to analyse the influence on the results of the assumed value for the electron density in the microwave discharge. As referred to above, we have considered $n_e(0) = 3 \times 10^{10}\,\mathrm{cm}^{-3}$ [9], which is in agreement with the value of the input microwave power $P = 300\,\mathrm{W}$ under the present conditions. However, the modifications on the concentrations of $N_2(A)$ metastables and $N(^4S)$ atoms as other values for $n_e(0)$ are considered in the discharge are reported in figure 9 for comparison.

3.2. Modifications of the reference model

In this section, we will justify the various assumptions made in the reference model and check the possibility of other explanations and reaction paths that could lead, in principle, to the growth of the $N_2(A\,^3\Sigma_u^+)$ metastable concentration and to the observed enhancement of the optical emissions in the afterglow.

In [9], a different explanation has been proposed for the growth profile of the $N_2(A)$ density in the SLA. According to that paper, up to the maximum of $[N_2(A)]$, at about $z = 19\,\mathrm{cm}$ or $t \sim 15\,\mathrm{ms}$, the density of $N_2(X\,^1\Sigma_g^+, v \geqslant 10)$ molecules is high enough to immediately induce reaction (9)
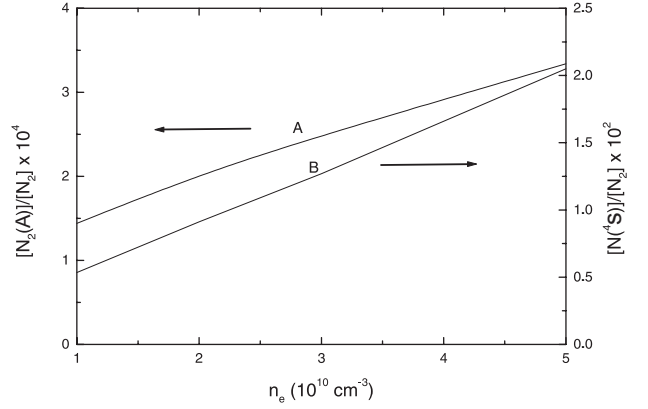
on $N(^2P)$ atoms, which are formed by quenching of $N_2(A)$ molecules by $N(^4S)$ atoms (reaction (8)) and then recycled to the metastable molecules. But, up to the minimum of $[N_2(A)]$, at about $z = 12\,\mathrm{cm}$ or $t \sim 5\,\mathrm{ms}$, the gas temperature is relatively high, so that the rate coefficient for three-body atomic recombination, leading in the first stage to $N_2(B\,^3\Pi_g)$ production, see reaction (19), but also allowing the production of $N_2(A)$ by radiative cascades, is low. Both $[N_2]$ and $[N(^4S)]$ concentrations are also smaller than at lower T_g. Thus, up to the attainment of the minimum around $t \sim 5\,\mathrm{ms}$, the rate for triplet state production by three-body atomic recombination is relatively low (10^{14} molecule $\mathrm{cm}^{-3}\,\mathrm{s}^{-1}$ as estimated in [9]). After $t \sim 5\,\mathrm{ms}$, the $N_2(A)$ density increases because the temperature reduction results in an enhancement of the rate coefficient for reaction (19) as well as of $[N_2]$ and $[N(^4S)]$ concentrations. At this region, the recycling of metastable molecules by $N(^2P)$ atoms and $N_2(X, v \geqslant 10)$ molecules is still effective. Finally, after the maximum of $[N_2(A)]$ at $z = 19\,\mathrm{cm}$, the decay of this concentration has been attributed to the continuous diminution of the concentration of $N_2(X, v \geqslant 10)$ molecules by V–T deactivation, mainly in collisions with $N(^4S)$ atoms, so that reaction (9) becomes less efficient for recycling the metastables $N_2(A)$.

Although, as pointed out in [9], this scenario alone cannot explain the magnitude of the maximum in the $N_2(A)$ concentration found in the SLA, it seems interesting to evaluate here the effect of such a set of reactions in the framework of a fully self-consistent model. Thus, in figures 10–12 we show a comparison between the measured concentrations of $N_2(A, v' = 0$–$6)$, $N_2(B)$ and $N_2^+(B)$ states, which we have reported above, and the results obtained using the present model for the following cases: (A) our reference case, with $k_{13} = k_{14} = 10^{-11}\,\mathrm{cm}^3\,\mathrm{s}^{-1}$, as in curves A of figures 1–3; (B) $k_{13} = k_{14} = 0$ and considering the rate coefficient of reaction (19) arbitrarily multiplied by a factor of 3; (C) $k_{13} = k_{14} = 10^{-11}\,\mathrm{cm}^3\,\mathrm{s}^{-1}$ and $3 \times k_{19}$; (D) $k_{13} = k_{14} = 0$, $3 \times k_{19}$ and $k_9 = 4 \times 10^{-11}\,\mathrm{cm}^3\,\mathrm{s}^{-1}$ as estimated in [9].

The rate coefficient used in this paper for reaction (19) is $k_{19} = 7.1 \times 10^{-33}\,\mathrm{cm}^6\,\mathrm{s}^{-1}$ at the lower temperature $T_g = 300\,\mathrm{K}$ [48], so that $3 \times k_{19}$ is of the order of the upper limit $2.25 \times 10^{-32}\,\mathrm{cm}^6\,\mathrm{s}^{-1}$ for the total rate coefficient deduced in [52]. On the other hand, the rate coefficient for the recycling reaction (9)

227
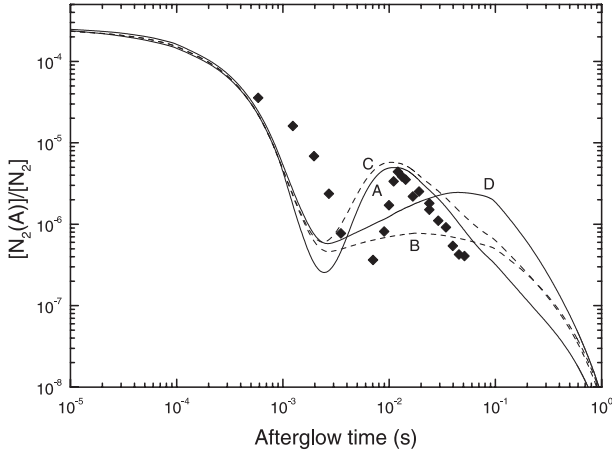
Figure 10. Temporal evolution of the fractional concentration of $N_2(A)$ metastables, under the conditions of figure 1, for the following cases: (A) $k_{13} = k_{14} = 10^{-11}$ cm^3 s^{-1} (reference case); (B) $k_{13} = k_{14} = 0$ and $3 \times k_{19}$ for the rate coefficient of three-body atomic recombination (see text); (C) $k_{13} = k_{14} = 10^{-11}$ cm^3 s^{-1} and $3 \times k_{19}$; (D) $k_{13} = k_{14} = 0$, $3 \times k_{19}$ and $k_9 = 4 \times 10^{-11}$ cm^3 s^{-1} [9]. The measured data are from [9, 12].
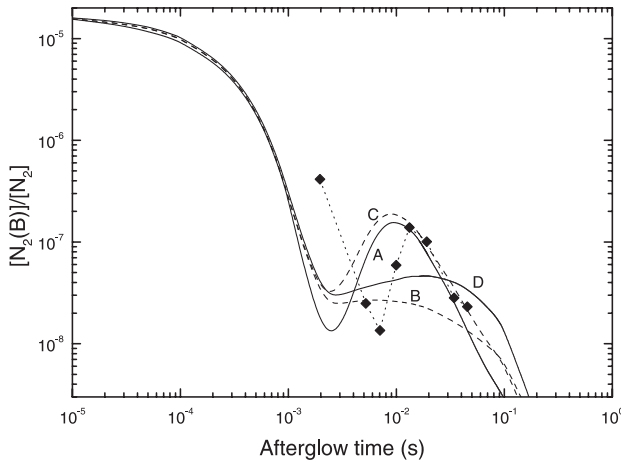
Figure 11. Fractional concentration of the $N_2(B)$ state for the same cases as in figure 10. Measured data taken from [13].
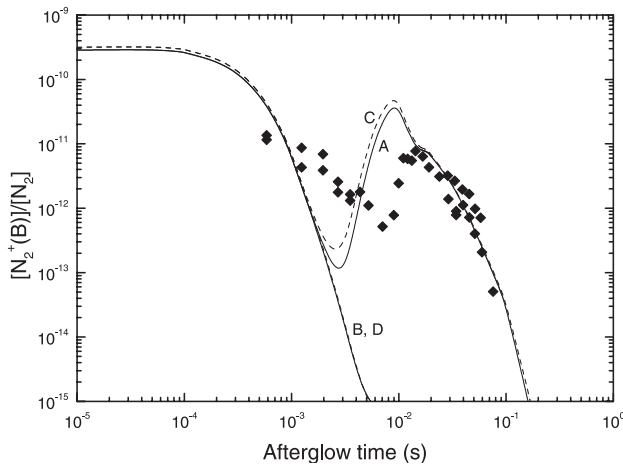
Figure 12. Fractional concentration of the $N_2^+(B)$ state for the same cases as in figure 10. Measured data taken from [13].
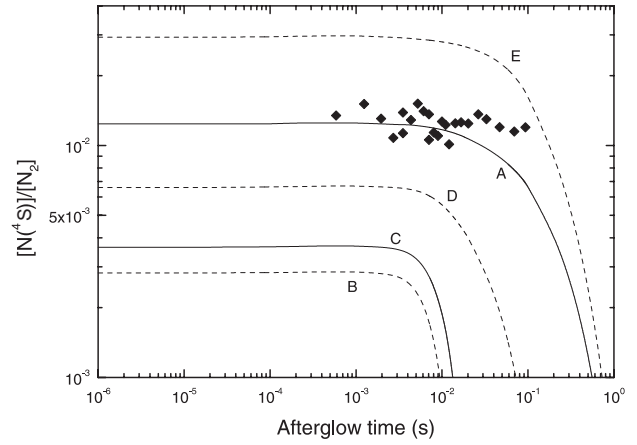
Figure 13. Fractional concentration of N(^{4}S) atoms for the following values of the rate coefficient of dissociation reaction (10) in cm^3 s^{-1}: (A) 1.5×10^{-12} (reference case); (B) 0; (C) 10^{-13}; (D) 5×10^{-13}; (E) 5×10^{-12}. Measured data are from [10].

used in this paper, $k_9 = 10^{-10} \times \exp(-1300/T_g)$ cm^3 s^{-1} [36], gives 2.7×10^{-11} cm^3 s^{-1} at $T_g = 1000$ K and 7.4×10^{-12} cm^3 s^{-1} at 500 K, which is almost an order of magnitude smaller than the value 4×10^{-11} cm^3 s^{-1} estimated in [9], based on a balance between reactions (8) and (9).

Figures 10–12 show that the conjoint action of the gas temperature decreases along the post-discharge, leading to an increase in the rate coefficient k_{19}, the increases in the concentrations of $[N_2]$ and $[N(^4S)]$, also due to the temperature decrease, and the diminution of the effectiveness of the recycling mechanism for $N_2(A)$ through reactions (8) and (9), cannot explain solely the appearance of the observed maxima in the afterglow as $k_{13} = k_{14} = 0$ (the cases of curves B and D). This is true even as the rate coefficients of reactions (9) and (19) are arbitrarily increased.

A second aspect to be considered here is the fact that there exists a lack of N(^{4}S) atoms and an excess of $N_2(A\,^3\Sigma_u^+)$ metastables predicted by the model, in comparison with the measurements realized in [9, 10], when electron impact dissociation is considered as the sole dissociation mechanism. This has led to the assumption that dissociation may also occur via reaction (10), involving collisions between vibrationally excited molecules $N_2(X\,^1\Sigma_g^+, v)$, at intermediate levels $15 \leqslant v \leqslant 19$, and $N_2(A)$ metastables [31]. Here, the rate coefficient of reaction (10) has been chosen as $k_{10} = 1.5 \times 10^{-12}$ cm^3 s^{-1} by fitting to the measured N(^{4}S) concentrations reported in [10].

In order to evaluate the sensitivity of the model to the rate coefficient of reaction (10), figures 13 and 14 show the fractional concentration of nitrogen atoms and metastables when different values are considered for k_{10} in the model: (A) 1.5×10^{-12} cm^3 s^{-1}; (B) 0; (C) 10^{-13} cm^3 s^{-1}; (D) 5×10^{-13} cm^3 s^{-1}; (E) 5×10^{-12} cm^3 s^{-1}. As shown in figure 13, the fractional concentration $[N(^4S)]/[N_2]$ increases from $\sim 2.8 \times 10^{-3}$ up to $\sim 1.2 \times 10^{-2}$, as the rate coefficient for reaction (10) varies from $k_{10} = 0$ (i.e. dissociation by electron impact only) to $k_{10} = 1.5 \times 10^{-12}$ cm^3 s^{-1} (our reference case). The agreement with the measured data is very satisfactory in this latter case. Regarding the fractional concentration $[N_2(A)]/[N_2]$ shown in figure 14, there occurs
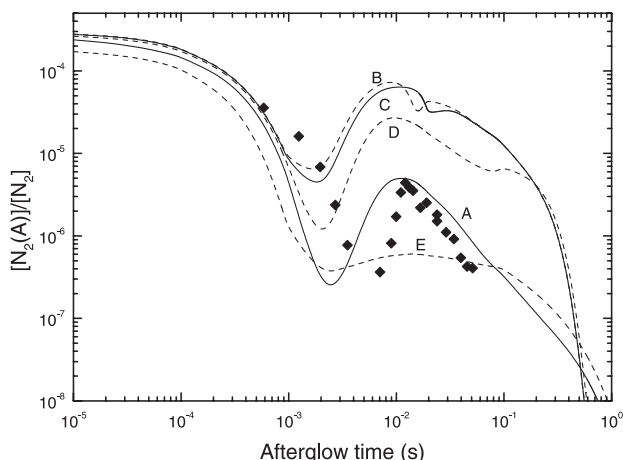
Figure 14. Fractional concentration of the $N_2(A)$ metastable for the same cases as in figure 13. Measured data taken from [9, 12].

Figure 15. Fractional concentration of the $N_2(A)$ metastable for the following assumptions of V–T rate coefficients in N_2–N collisions: (A) data reported in [42, 43] divided by 5, with transitions up to five quanta; (B) as in case A but assuming a division by 3; (C) as in case A but with division by 8; (D) data reported in [42, 43] with no corrections and assuming single quantum transitions only. Measured data taken from [9, 12].

a reverse tendency since the $N_2(A)$ population decreases not only as a result of the consumption through reaction (10) but, also to some lower extent, due to an enhancement of the quenching by N(^{4}S) atoms via reaction (8). In the case of the afterglow, another reason also exists for the small $[N_2(A)]$ concentration, which is the vibrational deactivation of $N_2(X\,^1\Sigma_g^+, v)$ molecules by V–T energy exchanges in N_2–N collisions leading to a small production of $N_2(A)$ via reaction (13).

Finally, it is worth concluding this section by showing the sensitivity of the model to the values of the rate coefficients for V–T processes associated with N_2–N collisions. These processes are of two types, a non-reactive mechanism, in which there just occurs a deactivation in the same sense as with N_2 molecules, and a reactive reaction with an exchange of the collision partner, i.e. through the reaction $N_2(X, v) + N \rightarrow (N_3) \rightarrow N + N_2(X, w)$, with $w < v$. The effect of an increase in the rate coefficients for these V–T processes is a much greater effectiveness of vibrational deactivation and consequently a diminution of the rates for $N_2(A)$ and $N_2(a')$ production by reactions (13) and (14).

Figures 15 and 16 show the relative concentrations in $N_2(A)$ and $N_2(B)$ states when different assumptions for these V–T rate coefficients are used in the model as follows: our reference rates obtained by reducing the values proposed in [42, 43] by a factor of 5 and assuming multi-quantum transitions up to five quanta (curves A); as in case A but by considering reductions by factors of 3 (curves B) and 8 (curves C) of data from [42, 43]; considering the same magnitude for the rate coefficients as reported in [42, 43] but assuming single quantum transitions only (curves D).

It is slightly difficult to infer unambiguously about the magnitude of the V–T rate coefficients in N_2–N collisions that should be used. However, this study shows that the V–T rates reported in [42, 43], together with the concentrations of N(^{4}S) atoms measured in [10], lead to too high rates for vibrational deactivation of the VDF, at the levels $v > 35$, thus avoiding the possibility that the V–V pumping-up process may occur. Here, we have seen that a reduction of the data [42, 43] by a factor of 5, with the assumption of multi-quantum transitions up to five quanta, allows that the pronounced maxima for the

Figure 16. Fractional concentration of the $N_2(B)$ state for the same cases as in figure 15. Measured data taken from [13].

concentrations of the various species in the SLA may occur. However, other values for the magnitude of the V–T rates combined with different assumptions for the number of v levels involved in a transition may be considered as well producing very similar effects.

4. Conclusions

This paper shows that the formation of the well-known short-lived (or pink) afterglow of nitrogen in the early flowing post-discharge can be explained as a result of near-resonant V–V energy exchange collisions leading to a pumping-up effect in the vibrational ladder. Although this fact has been already pointed out in our previous publications [14–16], this paper reports the final stage in these investigations in which an excellent agreement with experiment [9–13] has been achieved.

Basically, we state here that the metastables $N_2(A\,^3\Sigma_u^+)$ and $N_2(a'\,^1\Sigma_u^-)$ are produced in the afterglow by collisions

between N(^{4}S) atoms and highly vibrationally excited N$_2$(X $^1\Sigma_g^+$, $v > 35$) molecules, the latter being strongly overpopulated in the afterglow by the V–V pumping-up effect. This explanation is on the same lines as those proposed for other V–E energy transfer processes with CO(X $^1\Sigma^+$, v) [26, 27, 44] and NO(X $^2\Pi_r$, v) [28, 45] molecules. The present predictions for N$_2$(A $^3\Sigma_u^+$), N$_2$(B $^3\Pi_g$), N$_2^+$(B $^2\Sigma_u^+$) and N(^{4}S) concentrations are in good agreement with the measurements of the total N$_2$(A, $v' = 0$–6) concentration by intracavity laser absorption spectroscopy [8, 9, 12], the emission spectroscopy of 1$^+$ and 1$^-$ system bands of N$_2$ [13], and with the measured N(^{4}S) concentration by TALIF [10]. Moreover, the calculated VDFs of N$_2$(X $^1\Sigma_g^+$, v) molecules are in excellent agreement with the measurements at $v = 18$ [16] obtained by high sensitivity cavity ringdown spectroscopy in [11].

Here, we have considered that N(^{4}S) atoms are the long-lived species that collide on N$_2$(X $^1\Sigma_g^+$, v) molecules to produce the electronic metastables N$_2$(A $^3\Sigma_u^+$) and N$_2$(a$'$ $^1\Sigma_u^-$) in the afterglow. This assumption is a consequence of the long time-life of N(^{4}S) atoms and of the relatively small energy threshold for the excitation of the N(^{2}D) state. However, the possibility that the V–E energy transfer processes may also occur as a result of collisions of highly excited vibrational N$_2$ molecules with slow electrons, as is the case of energy transfer in CO laser pumped plasmas with the mechanism e($\epsilon + \Delta\epsilon$) + CO(X $^1\Sigma$, v) $\rightarrow$ e(ϵ) + CO(A $^1\Pi$, v') [27], should be questioned. As noted in [27], this effect in CO may occur at ionization degrees as low as $\sim$10^{-9}–10^{-7}.

This work is still in course both in Lisbon and Grenoble. There are projects to measure the VDF at higher v levels and the concentrations of molecular N$_2$(a$'$ $^1\Sigma_u^-$) and atomic N(^{2}P) metastables, as well as the population of N$_2^+$(X $^2\Sigma_g^+$) ions. On the other hand, the model will be improved by studying the effects of stepwise electron excitation processes in the first instants of the afterglow. The influence of electron superelastic collisions with N$_2$(A $^3\Sigma_u^+$) molecules on the EEDF will also be investigated to achieve a fully self-consistent solution of the electron and heavy particles in the nitrogen afterglow as outlined in [24].

Acknowledgments

References

[1] Ricard A, Oseguera-Pena J E, Falk L, Michel H and Gantois M 1990 *IEEE Trans. Plasma Sci.* **18** 940
[2] Kulisch W 1993 *Surf. Coat. Technol.* **59** 193
[3] Ohtani T, Ihashi N and Matsumoto O 2000 *Trans. Mater. Res. Soc. Japan* **25** 47
[4] Jama C, Dessaux O, Goudmand P, Soro J-M, Rats D and van Stebut J 1999 *Surf. Coat. Technol.* **116–119** 59

[5] Gaillard M, Raynaud P and Ricard A 1999 *Plasmas Polym.* **4** 241
[6] Moreau S, Moisan M, Tabrizian M, Barbeau J, Pelletier J, Ricard A and Yahia L' H 2000 *J. Appl. Phys.* **88** 1166
[7] Philip N, Saoudi B, Crevier M-C, Moisan M, Barbeau J and Pelletier J 2002 *IEEE Trans. Plasma Sci.* **30** 1429
[8] Foissac C, Campargue A, Kachanov A, Supiot P, Weirauch G and Sadeghi N 2000 *J. Phys. D: Appl. Phys.* **33** 2434
[9] Sadeghi N, Foissac C and Supiot P 2001 *J. Phys. D: Appl. Phys.* **34** 1779
[10] Mazouffre S, Foissac C, Supiot P, Vankan P, Engeln R, Schram D C and Sadeghi N 2001 *Plasma Sources Sci. Technol.* **10** 168
[11] Macko P, Cunge G and Sadeghi N 2001 *J. Phys. D: Appl. Phys.* **34** 1807
[12] Eslami E, Foissac C, Campargue A, Supiot P and Sadeghi N 2002 *Joint Conf. 16th Euro. Conf. on Atomic and Molecular Physics of Ionized Gases (ESCAMPIG)—5th Int. Conf. on Reactive Plasmas (ICRP) (Grenoble, France, 2002)* ed N Sadegi and H Sugai, p 57
[13] Eslami E, Campargue A, Foissac C, Supiot P and Sadeghi N 2003 *Frontiers in Low Temperature Plasma Diagnostics (FLTPD-V) (Villaggio Cardigliano, Specchia (Lecce) Italy, 2003)*
[14] Sá P A and Loureiro J 1997 *J. Phys. D: Appl. Phys.* **30** 2320
[15] Loureiro J, Sá P A and Guerra V 2001 *J. Phys. D: Appl. Phys.* **34** 1769
[16] Guerra V, Sá P A and Loureiro J 2003 *Plasma Sources Sci. Technol.* **12** S8
[17] Levaton J, Amorim J, Souza A R, Franco D and Ricard A 2002 *J. Phys. D: Appl. Phys.* **35** 689
[18] Beale G E Jr and Broida H P 1959 *J. Chem. Phys.* **31** 1030
[19] Supiot P, Dessaux O and Goudmand P 1995 *J. Phys. D: Appl. Phys.* **28** 1826
[20] Boisse-Laporte C, Chave-Normand C and Marec J 1997 *Plasma Sources Sci. Technol.* **6** 70
[21] Blois D, Supiot P, Barj M, Chapput A, Foissac C, Dessaux O and Goudmand P 1998 *J. Phys. D: Appl. Phys.* **31** 2521
[22] Supiot P, Blois D, De Benedictis S, Dilecce G, Barj M, Chapput A, Dessaux O and Goudmand P 1999 *J. Phys. D: Appl. Phys.* **32** 1887
[23] Guerra V, Sá P A and Loureiro J 2001 *Phys. Rev.* E **63** 046404
[24] Guerra V, Dias F M, Loureiro J, Sá P A, Supiot P, Dupret C and Popov Tsv 2003 *IEEE Trans. Plasma Sci.* **31** 542
[25] Treanor C E, Rich J W and Rehm R G 1968 *J. Chem. Phys.* **48** 1798
[26] Caledonia G E and Center R E 1971 *J. Chem. Phys.* **55** 552
[27] Plönjes E, Palm P, Rich J W, Adamovich I V and Urban W 2002 *Chem. Phys.* **279** 43
[28] Saupe S, Adamovich I, Grassi M J, Rich J W and Bergman R C 1993 *Chem. Phys.* **174** 219
[29] Guerra V and Loureiro J 1995 *J. Phys. D: Appl. Phys.* **28** 1903
[30] Slovetskii D I 1980 *Mechanisms of Chemical Reactions in Nonequilibrium Plasmas* (Moscow: Nauka)
[31] Guerra V, Galiaskarov E and Loureiro J 2003 *Chem. Phys. Lett.* **371** 576
[32] Guerra V, Tatarova E and Ferreira C M 2003 *Vacuum* **69** 171
[33] Sá P A, Loureiro J and Ferreira C M 1992 *J. Phys. D: Appl. Phys.* **25** 960
[34] Guerra V and Loureiro J 1997 *Plasma Sources Sci. Technol.* **6** 361
[35] Piper L G 1989 *J. Chem. Phys.* **90** 7087
[36] Vereshchagin K A, Smirnov V V and Shakhatov V A 1997 *Tech. Phys.* **42** 487
[37] Mankelevich Yu A, Pal' A F, Popov N A, Rakhimova T V and Filippov A V 2001 *15th Int. Symp. on Plasma Chemistry (ISPC) (Orléans, France, 2001)* ed A Bouchoule *et al*, p 1521
[38] Brovikova I N and Galiaskarov E G 2001 *High Temp.* **39** 809
[39] Galiaskarov E G, Brovikova I N and Bessarab A B 2000 *13th Int. Conf. on Gas Discharges and their Applications (GD) (Glasgow, UK, 2000)* ed S J MacGregor, p 663

[40] Piper L G 1989 *J. Chem. Phys.* **91** 864

[41] Zipf E C and MacLaughlin R W 1978 *Planet. Space Sci.* **26** 449

[42] Garcia E and Laganà A 1997 *J. Phys. Chem.* A **101** 4734

[43] Laganà A, de Aspuru G O and Garcia E 1996 Quasiclassical and quantum rate coefficients for the N + N$_2$ reaction, *Internal Report* Università degli Studi di Perugia, Dipartimento di Chimica

[44] Farrenq R, Rossetti C, Guelachvili G and Urban W 1985 *Chem. Phys.* **92** 389

[45] Dünnwald H, Siegel E, Urban W, Rich J W, Homicz G F and Williams M J 1985 *Chem. Phys.* **94** 195

[46] Guerra V and Loureiro J 1997 *Plasma Sources Sci. Technol.* **6** 373

[47] Kossyi I A, Kostinsky A Yu, Matveyev A A and Silakov V P 1992 *Plasma Sources Sci. Technol.* **1** 207

[48] Yamashita T 1979 *J. Chem. Phys.* **70** 4248

[49] Ricard A, Tétreault J and Hubert J 1991 *J. Phys. B: At. Mol. Opt. Phys.* **24** 1115

[50] Ricard A, Malvos H, Moisan M and Hubert J 1990 *8th Symp. on Elementary Processes and Chemical Reactions in Low Temperature Plasmas (Stará Lesná, Czechoslovakia)* ed P Lukác (Bratislava: Comenius University Press) p 212

[51] Kim Y C and Boudart M 1991 *Langmuir* **7** 2999

[52] Evenson K M and Burch D S 1966 *J. Chem. Phys.* **45** 2450